Nanophotonics and near field / Nanophotonique et champ proche

Light polarization properties of three fold symmetry gold nanoparticles: Model and experiments

Comportement à la polarisation optique de nanoparticules de symétrie d'ordre 3 : Modèle et résultats expérimentaux

Hong Shen [a], Jérémy Rouxel [a,b], Nicolas Guillot [c], Marc Lamy de la Chapelle [c], Timothée Toury [a,*]

[a] ICD-LNIO, UMR STMR CNRS 6279, université de technologie de Troyes, 12, rue Marie-Curie, 10000 Troyes, France
[b] Division of Chemistry and Biological Chemistry, School of Physical and Mathematical Sciences, Nanyang Technological University, 21 Nanyang Link, Singapore 637371, Singapore
[c] Laboratoire CSPBAT UMR 7244, université Paris 13, 74, rue Marcel-Cachin, 93017 Bobigny, France

A R T I C L E   I N F O

A B S T R A C T

In this study, we demonstrate that any complex nanostructure that belongs to C_n, with $n \geqslant 3$, symmetry point group for along at least one dimension displays apolar linear response to light input when the incoming wave vector is parallel to the C_n axis. Triangle and star shaped gold nanoparticles were designed and fabricated by electron beam lithography (EBL) technique. The apolar behavior of such nanostructures was experimentally confirmed by way of localized surface plasmon resonances (LSPR) properties and surface-enhanced Raman scattering (SERS) measurements.

© 2012 Académie des sciences. Published by Elsevier Masson SAS. All rights reserved.

R É S U M É

Dans cet article, nous démontrons que toutes les nanostructures, même de géométrie complexe, qui appartiennent au groupe de symétrie ponctuel C_n avec $n \geqslant 3$ ont une réponse optique linéaire ne dépendant pas de la polarisation de la lumière incidente, si son vecteur d'onde est parallèle à l'axe de symétrie C_n. Nous avons fabriqué des nanoparticules d'or en forme de triangle et d'étoile par lithographie électronique. Leur comportement apolaire est confirmé expérimentalement par des mesures sur les résonances plasmon et par diffusion Raman exaltée de surface.

© 2012 Académie des sciences. Published by Elsevier Masson SAS. All rights reserved.

1. Introduction

Over the past few years, gold plasmonic nanostructures have been exploited in many applications that may benefit from the excitation of localized surface plasmon resonance (LSPR) in the nanostructures. Together with the chemical stability and biocompatibility of gold, these plasmonic structures show potential in a wide variety of plasmon-resonance-based biosensors [1,2]. Therefrom, optical sensing techniques such as surface-enhanced Raman scattering (SERS) [3–6], surface-enhanced

---

* Corresponding author.
  E-mail address: toury@utt.fr (T. Toury).

resonance Raman scattering (SERRS) [7], surface-enhanced infrared absorption (SEIRA) [8,9], surface-enhanced fluorescence spectroscopy [10] have been intensively studied in recent years. For all plasmon-resonance-based sensors, the excitation of LSPR in metallic nanostructures plays the key role in the sensor sensitivity and performance. For example, a huge increase of the SERS signal could only be achieved at interstitial sites in nanoclusters or sharp edges of nanostructure surfaces due to enormous near-field enhancement [6,11–13]. However, LSPR excitations at so-called "hot spots" usually show strong dependence on the excitation polarization and as a consequence, SERS signals also display a dependence on the excitation polarization [11,14,15]. For example, the SERS measurements with nano-ellipses lead to intense Raman signals only when the excitation polarization is parallel to the major axis of the ellipses [15]. Such a highly sensitive polarization dependence of SERS behaviors brings limitations to actual sensing applications because rigorous management of polarization in the measurements set-up is then required to achieve the optimized enhancement factor. Cylinder (or spherical) shaped nanoparticles are apolar structures by virtue of their very nature and should therefore show an optical response that is insensitive to the excitation polarization. However, in such structures it is difficult to exploit efficiently all the physical processes involved in the field enhancement, such as the lightning rod effect which takes place at a surface with a small radius of curvature or in elongated structures such as nanorods, nanowires or tips [16]. The coupling of two approaching cylinders (or spheres) could indeed produce giant near-field enhancement at the tangential hot spot, but such coupling is then highly dependent on the polarization direction.

In this article, we will discuss on the design and fabrication of apolar nanostructures with an optical response insensitive to the light polarization. Such apolar plasmonic nanostructures are not limited to cylindrical or spherical shapes but could have a wide variety of shapes with sharp tips or coupled architectures that could give rise to "local hot spots" with giant near-field enhancement. We will demonstrate that with any complex nanostructure of a proper symmetry identity one can expect to get tuned LSPR spectral position, the most effective local field enhancement and apolar response in single nanostructure scheme.

2. Theoretical demonstration

We suggest a model to demonstrate why nanostructures with C_n symmetry ($n \geqslant 3$) exhibit an apolar behavior. This model is based on the assumption that the light is recorded in far field and linearly related to the incident electric field via a second-rank polarizability tensor α. It then obeys the intrinsic relationship $\mathbf{P} = \underline{\underline{\alpha}} \bullet \mathbf{E}$. Although the response of the particle is a near-field phenomenon, far-field observation and response homogeneity allow us to define a linear relationship.

The polarization vector is usually written in a Cartesian basis and the intrinsic relationship can thus be expressed by $P = \sum_{i,j} \alpha_{i,j} E_j e_i$. However, the Cartesian basis is not well adapted to treat easily problems involving rotational invariance. The irreducible (sometimes known as "spherical") tensor formalism [17,18] allows to handle such problems more efficiently and even suggest new shapes and symmetry features for linear and nonlinear applications [19]. In this formalism, each tensor will be decomposed as a direct sum of irreducible tensors of different rank J, each of these tensors abiding to canonical rotation properties with specific physical implication. For example, the second-rank tensor α can be represented as a direct sum of three irreducible tensors:

$$\alpha = \alpha^0 \oplus \alpha^1 \oplus \alpha^2 \tag{1}$$

- the trace α^0 with one component α^{00};
- the antisymmetric part α^1 with three components $\alpha^{1,\pm 1}$ and α^{10};
- the traceless symmetric part α^2 with five components $\alpha^{2,\pm 2}$, $\alpha^{2,\pm 1}$ and α^{20}.

The basis of irreducible tensors is isomorphic to a functional space spanned by spherical harmonics: each irreducible tensor α^J of rank J has $2J + 1$ components labeled α^{JM} with $-J \leqslant M \leqslant J$. Both spaces sustain irreducible representations of the rotation group SO(3) and thus transform via the Wigner $\mathcal{D}^J$ matrices [20]. In that way, the rotation properties of irreducible tensors are tabulated and drastic simplifications can be applied (e.g. selection rules that we get from group representation theory) or a priori complex statistical calculations of higher order nonlinear properties can be considerably reduced [21].

For the scalar ($J = 0$) and vector ($J = 1$) cases, the transformation from Cartesian to irreducible tensors is simple since there is a one-to-one correspondence. A scalar quantity is already as such an irreducible tensor and a Cartesian vector is related to an irreducible vector only by the following change of basis:

$$e_{\pm 1} = \mp \frac{1}{\sqrt{2}} (e_x \pm i e_y), \qquad e_0 = e_z \tag{2}$$

The components of the irreducible polarization are obtained by fully contracting the irreducible polarizabilities with an adequately defined tensor field. To select a component of the polarization, we introduce the read-out vector $\hat{e}$ which is a unit vector along the analyzer polarization [19]. The components in the spherical basis of the polarization are thus given by taking the following read-out tensor $\hat{e} = e_\mu$.

$$P^\mu = \alpha^0 \bullet \{E \otimes e_\mu\}^0 + \alpha^1 \bullet \{E \otimes e_\mu\}^1 + \alpha^2 \bullet \{E \otimes e_\mu\}^2 \tag{3}$$
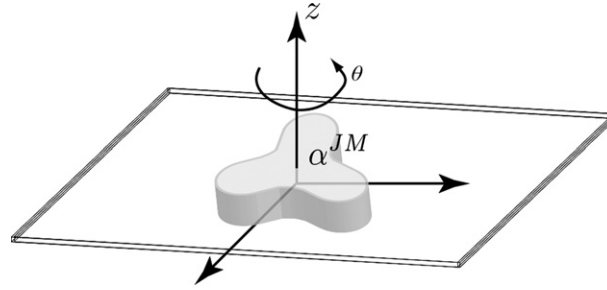
Fig. 1. Geometry of the nanoparticles and the local frame associated.

where $\{T^{j_1} \otimes U^{j_2}\}^J$ is the J part of the irreducible tensor product following angular momentum coupling rules using Clebsch–Gordan coefficients $C_{j_1 m_1, j_2 m_2}^{JM}$ [18]:

$$\{T^{j_1} \otimes U^{j_2}\}^{JM} = \sum_{m_1, m_2} C_{j_1 m_1, j_2 m_2}^{JM} T^{j_1 m_1} U^{j_2 m_2} \quad \text{for } |j_1 - j_2| \leqslant J \leqslant j_1 + j_2 \text{ and } -J \leqslant M \leqslant J \tag{4}$$

Under a rotation of θ around the normal axis shown in Fig. 1, the irreducible tensor transforms in a straightforward manner: $R_{(\theta,0,0)}[\alpha^{JM}] = \mathcal{D}^J(\theta,0,0)\alpha^{JM} = e^{iM\theta}\alpha^{JM}$ where $R_{(\Theta,\Psi,\Phi)}$ is the rotation operator parametrized by Euler angles and $e^{iM\theta}$ are the characters of the one-dimensional representations of the commutative planar rotation group. Let consider now a particle with C_n symmetry ($n \geqslant 3$). In this case, each component has to obey the following invariance equation: $\alpha^{JM} = e^{2\pi i \frac{M}{n}}\alpha^{JM}$. This relationship can be verified only if M is a multiple of 3. So, only $M = 0$ will be allowed and only components α^{00}, α^{10} and α^{20} of α do no vanish. They are connected to cylindrical symmetry. Since all these components are invariant by rotation around the z axis, the response of the particle is polarization independent:

$$\alpha = \alpha^{00} \oplus \alpha^{10} \oplus \alpha^{20} \tag{5}$$

Furthermore, α^{10} is also zero for a particle belonging to a C_{nv} or D_{nh} group since it corresponds to the antisymmetric part of the tensor which vanishes under reflection symmetries. A surviving α^{10} component would lead to a polarization rotation and would appear in the C_n group. Using Eq. (3), the response to a normally incident electric field is easily deduced by using numerical values of the Clebsch–Gordan symbol and $e_\mu = (-1)^\mu e_{-\mu}$:

$$P^1 = -E^1 \left(\frac{1}{\sqrt{3}}\alpha^{00} - \frac{1}{\sqrt{2}}\alpha^{10} + \frac{1}{\sqrt{6}}\alpha^{20} \right) \tag{6}$$

$$P^0 = 0 \tag{7}$$

$$P^{-1} = -E^{-1} \left(\frac{1}{\sqrt{3}}\alpha^{00} + \frac{1}{\sqrt{2}}\alpha^{10} + \frac{1}{\sqrt{6}}\alpha^{20} \right) \tag{8}$$

The polarization field is then parallel to the incident electric field when $\alpha^{10} = 0$ and their magnitudes are related by:

$$\|P\| = \|E\| \left[\left(\frac{1}{\sqrt{3}}\alpha^{00} + \frac{1}{\sqrt{6}}\alpha^{20} \right)^2 - \frac{1}{2}(\alpha^{10})^2 \right] \tag{9}$$

To summarize, we have shown that a particle belonging to a C_n ($n \geqslant 3$) group exhibits an apolar polarization response. Moreover, if the particle belongs to C_{nv} or D_{nh} groups, the polarization is parallel to the incoming electric field.

3. Experiments and results

As discussed above, a nanostructure that belongs to C_n, with $n \geqslant 3$, symmetry point group along at least one scale has an optical response that is insensitive to the light polarization when the wave vector is parallel to the C_n axis. The apolar behavior of such nanostructures was experimentally verified in the case of the LSPR properties and near-field enhancement observed by SERS measurements. In the LSPR measurements both real and imaginary parts of α are involved in the extinction response: absorption is related to the imaginary part and diffusion is related to the modulus. For the SERS measurements, the nanoparticles act as a resonator for the electromagnetic field (efficiency related to α) and the molecules on the nanoparticles are involved in the Raman scattering.

Triangle and star shaped nanoparticles of a C_{3v} symmetry were designed and fabricated by electron beam lithography (EBL) which was achieved by a 30 kV Hitachi S-3500N scanning electron microscope (SEM) equipped with a nanometer pattern generation system (NPGS) [15]. To realize EBL, the glass substrate was coated with a high resolution resist (PMMA) with 10 nm of aluminum on the top to make the surface conductive. Then the sample was loaded in the SEM chamber to "expose" the designed patterns with the electron beam. After exposure, the patterns were developed using
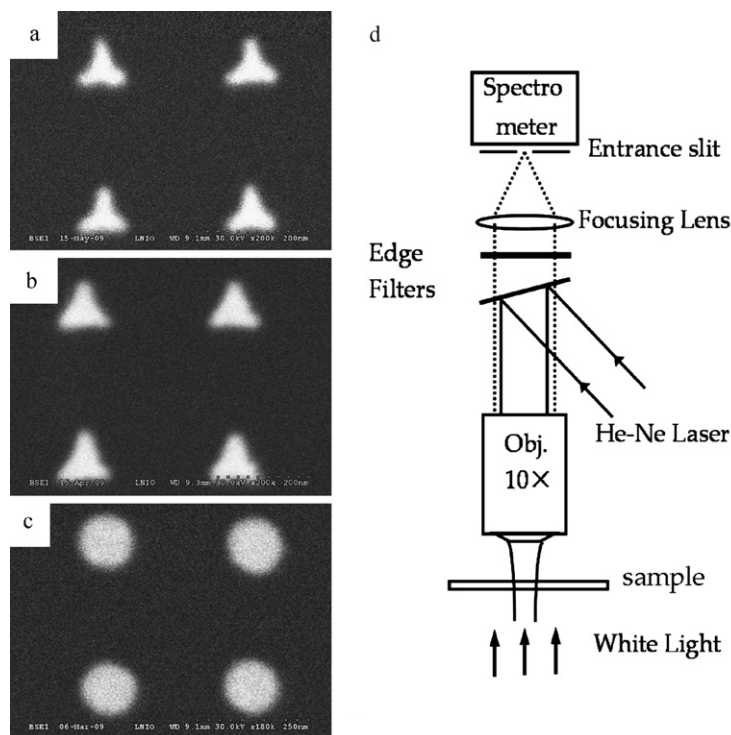
Fig. 2. SEM images of nano-stars (a), nano-triangles (b) (length: 100 nm) and nano-cylinders (c) (diameter: 125 nm); Experimental set-up for extinction and SERS measurements (d): extinction spectrum is recorded in transmission configuration with a ×10 objective (N.A. = 0.25) by removing the edge filters; Raman spectroscopy is recorded with a ×100 objective (N.A. = 0.90) in backscattering geometry.

methylisobutylketone (MIBK):isopropyl alcohol (IPA) 1:3 and then the desired mass thickness of gold is evaporated on the sample. After lift-off in acetone, the shape and the lateral sizes of the nanoparticles were checked by using SEM (Hitachi S-3500N) operating in BSE (backscattered electron) mode. Thanks to the precise control on the particle shape and size of EBL technique, well shaped nano-stars and triangles with perfect C_{3v} symmetry were obtained, as shown in Figs. 2(a)–(b), each have a side length of 100 nm, out-of-plane height of 50 nm. The gap between adjacent particles has been kept constant at 200 nm because at such a distance any near-field coupling could be neglected.

Extinction and SERS measurements were performed with a Jobin-Yvon micro-Raman spectrophotometer (Labram) (Fig. 2(d)). The extinction spectra were recorded in transmission configuration with a ×10 objective (N.A. = 0.25) by removing the edge filters. To achieve SERS measurements, the substrates were immersed in a 10^{-3} M solution of trans-1,2-bis(4-pyridyl)ethylene (BPE) during 1 h and dried with nitrogen. Raman measurements are carried out with the 632.8 nm line of a He–Ne laser, and Raman spectroscopy was recorded with a ×100 objective (N.A. = 0.90) in backscattering geometry.

Fig. 3 gives the comparison of LSPR properties on nano-cylinders and nano-stars. A nano-cylinder is an intrinsically apolar structure which should show optical response insensitive to the excitation polarization. However, in such structure the tuning of LSPR is not so "efficient": as shown in Fig. 3(a), to tune the plasmon resonance between 700 and 800 nm requires the diameters of Au nano-cylinders to increase from 150 to 260 nm, however, for nano-stars of the same height, the size varies from 100 to 150 nm. It is worthy to mention that to get the most efficient near-field enhancement one phenomenon could not be neglected: the "lightning rod effect", in which the confinement of the charges at a surface with a small radius of curvature makes an additional enhancement factor. Such effect takes place in very small nanostructures or in elongated nanostructures such as nanorods, nanowires or tips. Thus, in the case of spherical or cylindrical Au nanoparticles of large diameters (above 150 nm), the lightning rod effect could be ignored because of too large curvature. This means in such structures one could not get the maximal near-field enhancement at any plasmon resonance wavelength. As demonstrated in Fig. 3(b), to get a plasmon resonance at 790 nm requires the nano-cylinders and nano-stars to have a size of 260 nm and 150 nm (both have the same height), respectively. However, the nano-stars show a much thinner LSPR line width than that observed from the nano-cylinders. A thinner LSPR indicates a higher local field enhancement [22,23] which benefits from the smaller size and sharp tip of the nano-stars.

To characterize the apolar behavior of different nanostructures, extinction spectra were recorded with incident polarization varied continuously in the sample plane. The LSPR position as a function of the polarization angle (Fig. 4) presents a few changes for nano-stars, nano-triangles and nano-cylinders. As shown in Fig. 5, the range of LSPR shift under polarization rotation for all the triangle and star shaped particles, regardless of particle size, is comparable to or even smaller than that
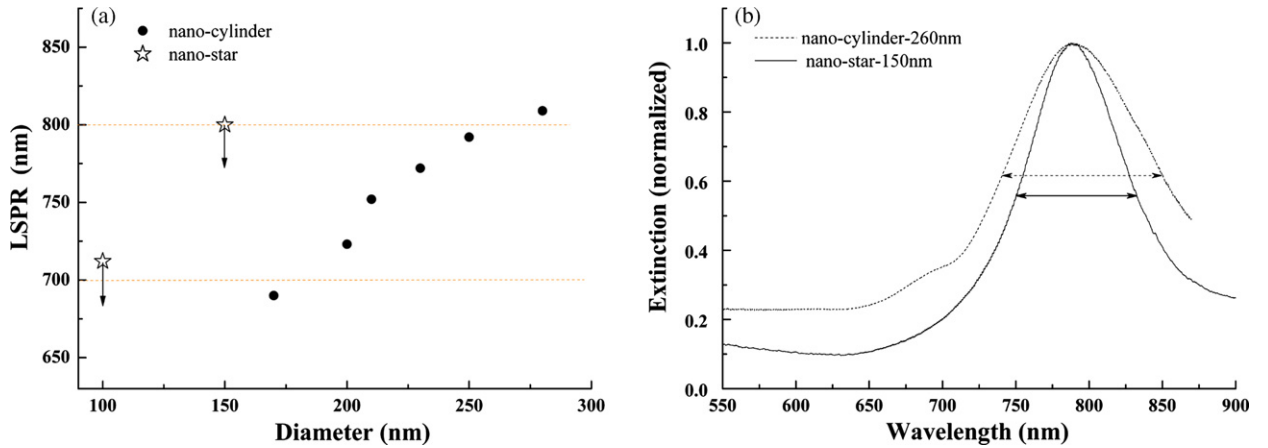
Fig. 3. (a) Evolution of the localized surface plasmon resonance (LSPR) position versus the nano-cylinder diameter (dot) and nano-star side length (star) (both have a height of 50 nm). (b) Extinction spectra of gold nano-cylinders (diameter: 260 nm, height: 50 nm) (dashed line) and gold nano-stars (side length: 100 nm, height: 50 nm) (solid line): each has a resonance peak at 790 nm, the values of the full width at half maximum (FWHM) are 110 nm and 83 nm respectively for nano-cylinders (dashed arrow) and nano-stars (solid arrow).
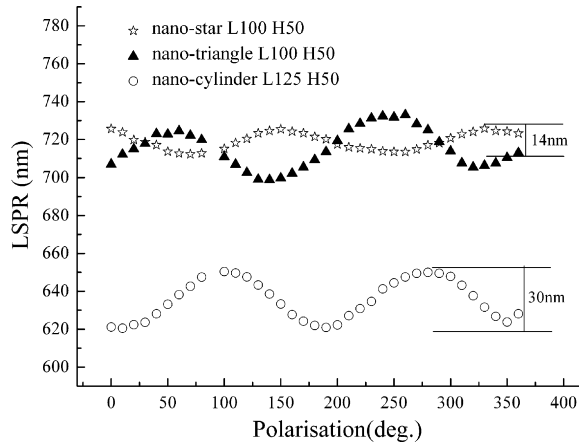
Fig. 4. LSPR position versus incidence polarization angle for nano-stars (star), nano-triangles (triangle) (length: 100 nm, height: 50 nm), and nano-cylinders (circle) (diameter: 125 nm, height: 50 nm).

Shape \ Height (nm)		λ_{LSPR}(average) [$\Delta\lambda$] (nm)		I_{LSPR}(nor/ave): $\pm\sigma$, [max/min]		FWHM: $\pm\sigma$, [max/min]	
		50	80	50	80	50	80
Cylinder (D=125nm)	●	636 [30]		±0.13 [1.3]		±0.04 [1.1]	
Ellipse (L=80 W=40 nm)	▬	675		±0.94 [32]			
Triangle (L=105 nm)	▲	720 [30]	704 [18]	±0.26 [2.7]	±0.13 [1.8]	±0.11 [1.3]	±0.03 [1.1]
Star (L=100)	✦	718 [15]	710 [12]	±0.24 [2.4]	±0.10 [1.2]	±0.16 [1.4]	±0.06 [1.1]

Fig. 5. LSPR properties of nanostructures under polarization rotation for four different shapes and two heights (50 nm and 80 nm): LSPR position with its maximum variation between square brackets; standard deviation of the LSPR intensity with the ratio of the maximum to the minimum LSPR intensity between square brackets; standard deviation of the line width (full width at half maximum, FWHM) with the ratio between the maximum and minimum FWHM between square brackets.
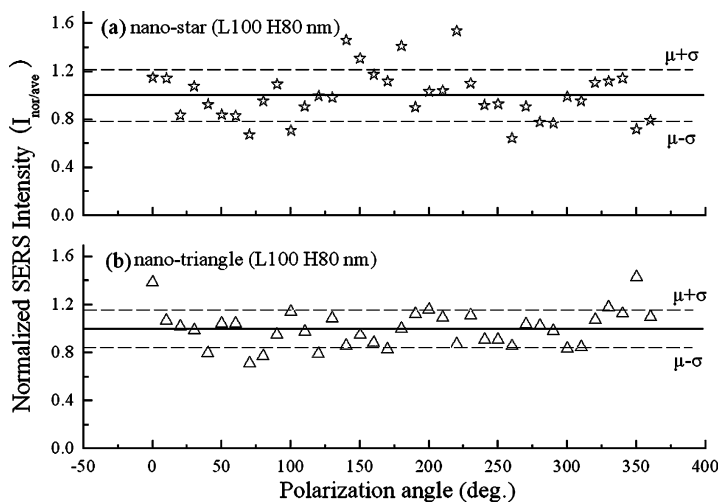
Fig. 6. SERS intensity (normalized by average value) versus incidence polarization angle for nano-stars (a) and nano-triangles (length: 100 nm, height: 80 nm), standard deviations around the average value are indicated in the figure ($\sigma = 21\%$ for nano-star and $\sigma = 15.7\%$ for nano-triangle).

observed for the nano-cylinders whereas such structures are intrinsically apolar. For example, the LSPR shift for the nano-triangles ($L = 105$ nm, $H = 80$ nm) is only about 20 nm. Such a shift corresponds to a size drift around 15 nm which is almost the resolution of EBL fabrication. Thus, the observed LSPR shift is not due to polarization dependence or to other specific physical processes but only to size drift or shape deviation appearing during the EBL process because of technical uncertainties.

More interestingly, as given in Fig. 5, both the intensity and line width (full width at half maximum, FWHM) of the LSPR are nearly independent of the polarization angle except the ellipses in which the LSPR intensity decreases almost down to zero for a polarization perpendicular to its major axis. The nearly constant LSPR intensity and line width indicate a constant LSPR excitation, as well as a highly efficient near-field enhancement by the polarized light. To estimate the variation of LSPR under the polarization rotation, the standard deviation around the average value was calculated for both the intensity and line width. The standard deviation for LSPR intensity is under 30% for all the nano-triangles and nano-stars and even smaller deviation is obtained for the LSPR line width, which reveal a fairly constant near-field enhancement with respect to polarized excitation.

To verify the apolar near-field enhancement of such nanostructures, we performed the SERS measurements with the nano-triangles and nano-stars of 80 nm height because they show smaller deviations for LSPR intensity and line width under polarization rotation. The SERS intensity (trans-1,2-bi-(4-pyridyl)ethylene (BPE) band at 1200 cm^{-1}) as a function of the polarization angle is shown in Figs. 6(a) and (b) for nano-stars and nano-triangles, respectively. As for the LSPR intensity, we have calculated the standard deviation for the SERS intensity around the average value as indicated in Fig. 6. The larger deviation of SERS intensity for nano-stars could be explained by the wider shape distribution for nano-stars than that for nano-triangles appearing during EBL fabrication. However, the deviation under 20% is perfectly acceptable for sensor applications and such deviation can be explained by the LSPR deviation and then is due to the imperfections of the nanostructures from lithography process and not from apolar considerations. The results of SERS measurements confirm that such nanostructures display apolar behavior in the near field.

Thus the theoretical model was perfectly verified by the extinction and SERS measurements, thus confirming that any complex nanostructures with a C_n symmetry (with $n \geqslant 3$) have apolar behaviors both in far field and near field. The apolar structures are not limited to spherical or cylindrical particles but can exhibit sharp tips provided they include a proper symmetry axis with an order $n \geqslant 3$. This model could also be generalized to coupled architectures that could provide "local hot spots" with giant near-field enhancement as long as the symmetry identity is satisfied for the whole architecture. The coupled architectures could, for example, be trimers or any higher multimers of nanoparticles including periodically distributed nanoparticles around a central axis.

4. Conclusion

Based on group theory, we demonstrated that any complex nanostructure that abides to the C_n, with $n \geqslant 3$, symmetry point group along at least one scale acts as an apolar system for any optical excitation with a wave vector parallel to that direction. The model was clearly confirmed by the experimental results with respect to the LSPR properties and near-field enhancement as observed by SERS measurements. Nearly constant LSPR and SERS intensity with small deviations were observed for triangle and star shaped nanoparticles of a C_{3v} symmetry. Moreover, the observed LSPR and SERS intensity deviations are due to the imperfections of the nanostructures as from the lithography process and can be largely reduced

by improving the fabrication process. Such apolar structure could be extended to coupled architectures that could give rise to "local hot spots".

Acknowledgements

References

[1] E. Hutter, J. Fendler, Exploitation of localized surface plasmon resonance, Adv. Mater. 16 (19) (2004) 1685–1706.

[2] W. Fritzsche, T.A. Taton, Metal nanoparticles as labels for heterogeneous, chip-based DNA detection, Nanotechnology 14 (12) (2003) R63.

[3] S. Nie, S.R. Emory, Probing single molecules and single nanoparticles by surface-enhanced Raman scattering, Science 275 (5303) (1997) 1102–1106, http://dx.doi.org/10.1126/science.275.5303.1102.

[4] A.J. Haes, R.P. Van Duyne, A nanoscale optical biosensor: Sensitivity and selectivity of an approach based on the localized surface plasmon resonance spectroscopy of triangular silver nanoparticles, J. Am. Chem. Soc. 124 (35) (2002) 10596–10604, pMID: 12197762, http://dx.doi.org/10.1021/ja020393x.

[5] H. Xu, J. Aizpurua, M. Käll, P. Apell, Electromagnetic contributions to single-molecule sensitivity in surface-enhanced Raman scattering, Phys. Rev. E 62 (2000) 4318–4324, http://dx.doi.org/10.1103/PhysRevE.62.4318.

[6] K. Kneipp, Y. Wang, H. Kneipp, L.T. Perelman, I. Itzkan, R.R. Dasari, M.S. Feld, Single molecule detection using surface-enhanced Raman scattering (SERS), Phys. Rev. Lett. 78 (9) (1997) 1667–1670, http://dx.doi.org/10.1103/PhysRevLett.78.1667.

[7] K.-i. Yoshida, T. Itoh, H. Tamaru, V. Biju, M. Ishikawa, Y. Ozaki, Quantitative evaluation of electromagnetic enhancement in surface-enhanced resonance Raman scattering from plasmonic properties and morphologies of individual Ag nanostructures, Phys. Rev. B 81 (2010) 115406, http://dx.doi.org/10.1103/PhysRevB.81.115406.

[8] F. Neubrech, A. Garcia-Etxarri, D. Weber, J. Bochterle, H. Shen, M.L. de la Chapelle, G.W. Bryant, J. Aizpurua, A. Pucci, Defect-induced activation of symmetry forbidden infrared resonances in individual metallic nanorods, Appl. Phys. Lett. 96 (21) (2010) 213111, http://dx.doi.org/10.1063/1.3437093.

[9] A. Pucci, F. Neubrech, D. Weber, S. Hong, T. Toury, M.L. de la Chapelle, Surface enhanced infrared spectroscopy using gold nanoantennas, Phys. Status Solidi (b) 247 (8) (2010) 2071–2074, http://dx.doi.org/10.1002/pssb.200983933.

[10] C.D. Geddes, I. Gryczynski, J. Malicka, Z. Gryczynski, J.R. Lakowicz, Metal-enhanced fluorescence: Potential applications in HTS, Comb. Chem. High Throughput Screen. 6 (2003) 109–117.

[11] H. Xu, E.J. Bjerneld, M. Käll, L. Börjesson, Spectroscopy of single hemoglobin molecules by surface enhanced Raman scattering, Phys. Rev. Lett. 83 (1999) 4357–4360, http://dx.doi.org/10.1103/PhysRevLett.83.4357.

[12] E. Prodan, C. Radloff, N.J. Halas, P. Nordlander, A hybridization model for the plasmon response of complex nanostructures, Science 302 (5644) (2003) 419–422, http://dx.doi.org/10.1126/science.1089171.

[13] C.E. Talley, J.B. Jackson, C. Oubre, N.K. Grady, C.W. Hollars, S.M. Lane, T.R. Huser, P. Nordlander, N.J. Halas, Surface-enhanced Raman scattering from individual Au nanoparticles and nanoparticle dimer substrates, Nano Lett. 5 (8) (2005) 1569–1574, http://dx.doi.org/10.1021/nl050928v.

[14] K.-i. Yoshida, T. Itoh, H. Tamaru, V. Biju, M. Ishikawa, Y. Ozaki, Quantitative evaluation of electromagnetic enhancement in surface-enhanced resonance Raman scattering from plasmonic properties and morphologies of individual Ag nanostructures, Phys. Rev. B 81 (2010) 115406, http://dx.doi.org/10.1103/PhysRevB.81.115406.

[15] J. Grand, M.L. de la Chapelle, J.-L. Bijeon, P.-M. Adam, A. Vial, P. Royer, Role of localized surface plasmons in surface-enhanced Raman scattering of shape-controlled metallic particles in regular arrays, Phys. Rev. B 72 (3) (2005) 033407, http://dx.doi.org/10.1103/PhysRevB.72.033407.

[16] A. Wokaun, Surface Plasmons on Smooth and Rough Surfaces and on Gratings, vol. 38, Academic Press, New York, 1984.

[17] J. Jerphagnon, D. Chemla, R. Bonneville, The description of the physical properties of condensed matter using irreducible tensors, Adv. Phys. 27 (1978) 609.

[18] D. Varshalovich, A. Moskalev, V. Khersonskii, Quantum Theory of Angular Momentum, World Scientific Pub. Co. Inc., 1988.

[19] J. Zyss, Molecular engineering implication of rotational invariance in quadratic nonlinear optics: From dipolar to octupolar molecules and materials, J. Chem. Phys. 98 (1993) 6583.

[20] M.E. Rose, Elementary Theory of Angular Momentum, Dover, 1957.

[21] S. Brasselet, J. Zyss, Multipolar molecules and multipolar fields: probing and controlling the tensorial nature of nonlinear molecular media, J. Opt. Soc. Am. B 15 (1998) 257.

[22] T. Klar, M. Perner, S. Grosse, G. von Plessen, W. Spirkl, J. Feldmann, Surface-plasmon resonances in single metallic nanoparticles, Phys. Rev. Lett. 80 (1998) 4249–4252, http://dx.doi.org/10.1103/PhysRevLett.80.4249.

[23] S.A. Maier, Plasmonics: Fundamentals and Applications, Springer-Verlag, New York, 2007.